Study of grasp-energy based optimal distribution of contact forces on a humanoid robotic hand during object grasp

Sourajit Mukherjee ⬢, Abhijit Mahapatra*⬢, Amit Kumar and Avik Chatterjee

Advanced Design and Analysis Group, CSIR-Central Mechanical Engineering Research Institute, Durgapur 713209, India
*Corresponding author. E-mail: abhi.mahapatra@gmail.com

Abstract

A novel grasp optimization algorithm for minimizing the net energy utilized by a five-fingered humanoid robotic hand with twenty degrees of freedom for securing a precise grasp is presented in this study. The algorithm utilizes a compliant contact model with a nonlinear spring and damper system to compute the performance measure, called 'Grasp Energy'. The measure, subject to constraints, has been minimized to obtain locally optimal cartesian trajectories for securing a grasp. A case study is taken to compare the analytical (applying the optimization algorithm) and the simulated data in MSC.Adams®, to prove the efficacy of the proposed formulation.

1. Introduction

Grasping and manipulation pose one of the most complex challenges in robotics. Therefore, in the present study, humanoid hand-type gripper is chosen over simpler grippers which have lesser degrees of freedom (DoFs) in their fingers/jaws, so that small objects can be grasped and dexterously manipulated. Grippers in the form of a humanoid hand have the advantage of being very articulate end effectors. Due to the multiple DoFs available in the fingers, they can easily adapt to hold objects of complex shapes securely. They can also be easily utilized to perform various types of grasps, such as pinch and power grasps. As a matter of consequence, grasping an object with the appropriate type of grasp can lead to the utilization of a lesser number of fingers. Also, such grippers have redundant DoFs in their fingers which is one of the major advantages over simple grippers. Redundancy resolution in such fingers offers opportunities for singularity avoidance, as well as trajectory optimization by the implementation of the proper performance criteria. Based on the findings and definitions of studies detailing human hand behaviors and the complexity of robotic grasping, the object manipulation by humanoid hand in the present study has been divided into three phases: I. the 'Approach' phase, II. the 'Contact' phase, and III. the 'Grasp' phase [1, 2]. The time between the start of finger motion and the instant before contact is the Approach phase. The instant at which the links come in contact with the object is the Contact phase, and it is followed by the Grasp phase that exists until the object is held securely by the gripper. Figure 1 shows a finger going through the various phases of grasping an object, with each phase highlighted. It is to be noted that the Contact phase is assumed to exist for only a single instant, since it is considered as a Transition phase. However, the Contact phase is the most important phase, as it deals with the transition between the Approach and Grasp phases. The joint configuration of the fingers at the Contact phase will decide their joint-space trajectories in both the Approach and Grasp phases. Depending on the number of contact points, each finger considers a different inverse kinematics (IK) algorithm, which is described in later sections.
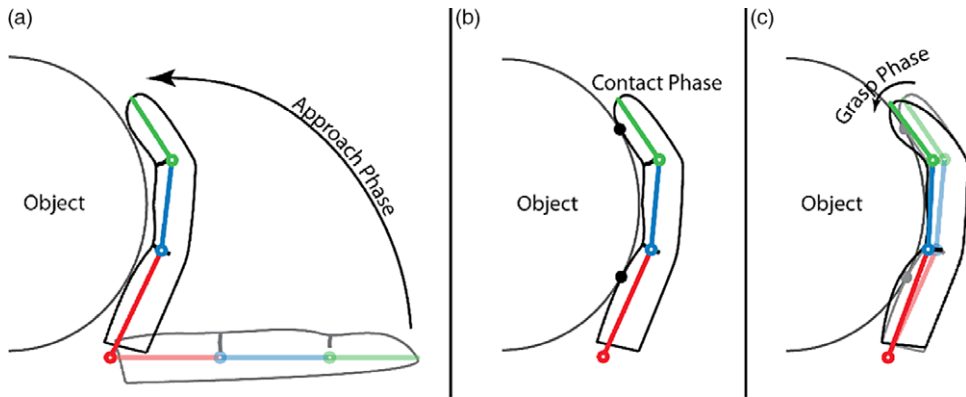
Figure 1. *Schematic representation of a finger-object interaction during various phases of a grasp.*

In the present study, the total energy required by all the fingers of a gripper to firmly grasp an object during the Grasp phase has been termed as 'Grasp Energy', which is to be minimized using optimization techniques by selecting optimal contact parameters. The contact parameters have been determined based on the nonlinear spring and damper contact model. The study also takes into consideration Marhefka and Orin's compliant contact model [3] and the static friction pyramid [4] to determine the normal contact forces and the frictional forces, respectively. The optimal contact parameters are used to generate the Grasp phase and Approach phase trajectories. Thereafter, the trajectory requiring the minimum total torque is selected. The assumptions in the present study are as follows:

1. Each robotic finger is treated as an independent serial articulated mechanism.
2. All the links of the finger and the grasping object are rigid except at the point of contact where there is compliancy.
3. All colliding surfaces are nonconforming with respect to each other.
4. Each link of a finger contacts the object at a single point.
5. No rebound on impact.
6. The object coordinates and orientation are invariant, with respect to the world fixed reference frame, during the entire grasp.

The paper is organized as follows: Section 2 includes a brief overview of the previous studies. Section 3 gives a brief description of the anatomy of the human hand. Next, the IK for the Contact phase is derived in Section 4 followed by Grasp-Energy optimization modeling in Section 5. Using the derivations carried out in Sections 4 and 5, the inverse kinematic trajectory generation for the Grasp and Approach phases is detailed in Section 6. Simulation results and comparison with MSC.ADAMS® data are stated and discussed in Section 7 with some conclusions drawn in Section 8.

2. Review of Previous Work

One of the major challenges in designing an articulated mechanism targeting object grasp is the optimization of its motion using a desirable performance index. Each approach to optimization uniquely depends on the application itself and the number of allied parameters taken into account.

In redundant manipulators, where the degrees of freedom in the task space are lesser than those in the joint space, the inverse kinematic (IK) equations for a given task space position and/or orientation can have an infinite number of solutions. Suh and Hollerbach [5], worked on an algorithm, optimizing the inverse kinematic solution using the dynamic manipulability index. The result of such a kinematic

resolution was later minimized using null-space damping, as presented by Kang and Freeman [6]. They used local torque optimization methods that are usually computationally faster than global optimization methods, but may lead to compounding errors over many time steps as studied by Hollerbach and Suh [7]. Dubey *et al.* [8] used a 'desired velocity' vector for optimizing the motion of a 7-DoF robotic arm with spherical wrist, using the gradient projection method which was a local optimization method. Tsai and Kohli [9] proposed a kinematic scheme for planning manipulator trajectory, based on the polynomial expansions of forward kinematic equations. Gorce *et al.* [10] described a control/command approach for multifinger mechanisms, where low-level and high-level commands were implemented together, to control the fingers of a multifingered gripper. Bakhy [11] mathematically modeled the contact pressure distribution at contact zone with hemi-cylindrical fingers with rolling contact constraints. Jeong *et al.* [12] mapped the force distribution between fingers for common grasps, using a film-type force sensor. Jo and Bae [13] later used the data to design an exoskeleton, driven by series elastic actuators.

The two-norm of manipulator torques is an important performance measure for local torque optimization methods. Kang [14] used this measure to derive the equations for optimal force and joint torque distribution among multiple redundant manipulators holding the same object. One limitation of this optimization scheme was that the author only considered equality constraints, similar to that carried out by Kang and Freeman [6] (static equilibrium between joint torques and external forces) to derive the force distribution equations, using Lagrangian multipliers. Cheng and Orin [4] proposed a formulation for optimizing force distribution using linearized friction constraints. Inequality constraints, namely the geometric constraints for joint motion, were later incorporated by Zhang *et al.* [15]. However, the authors only utilized kinematic inequality constraints to solve the optimization problem.

In another method, it was observed that optimizing joint torques for multiple coordinating articulated serial mechanisms involves selection of an optimal external force vector acting on the manipulator. Based on that, Klein and Kittivatcharapong [16] used the gradient projection method to determine the optimal force distribution for each leg of a legged/walking robot, subject to friction-cone constraints. Buss *et al.* [17] further used this method for optimization of the grasp force matrix, to balance the force of an external object grasped by a *N*-fingered hand. Dai and Kerr [18] proposed analyzing indeterminate grasps by utilizing elasticity constraints at contact points to determine the force distribution among the fingers performing the grasp. Suhaib *et al.* [19] followed a more geometric approach for grasp force optimization by identifying various grasp planes to maximize the friction cone angle. However, it was an unconstrained optimization technique. Jia *et al.* [20] used the volumes of the generalized external and internal contact force ellipsoids to establish an optimal grasp planning method.

Further studies dealt with optimizing the grasp configuration itself. Yu *et al.* [21] worked on a procedure for determining the optimal power grasp form, given a set of known contact points. Horowitz and Burdick [22] presented an algorithm for treating the tasks of arm trajectory planning, grasp planning, contact force optimization, and object manipulation as a single problem. Dong *et al.* [23] analyzed the grasp stability of precision grasps, using a force-form based analysis, to optimize the design of an underactuated two-finger gripper. Fan and Tomizuka [24] introduced a grasp planning framework that used multidimensional surface fitting and a corresponding grasp trajectory optimization algorithm for grasping complex objects.

Many authors opted for optimization in the design stage itself, to obtain better performance of the developed robotic grippers. Müller *et al.* [25] describe several approaches for the design of a soft robotic gripper including selection of the appropriate model for characterization of the maximum payload on the gripper, material characterization, and simulation of grasp to determine its performance at various loads. Kim *et al.* [26] developed a Deep-Neural-Network-based algorithm to identify optimal grasping points based on an object's geometric features for obtaining a stable grasp. Researchers from the University of Brazil developed an anthropometric robotic hand gripper, the UnB-Hand [27], which was designed with bio-inspired optimization algorithms, and was proven to be able to successfully perform grasps according to the Cutkosky grasping taxonomy, that is, power and precision grasps necessary for machining operations. Elangovan *et al.* [28] proposed a novel adaptive gripper that can adjust link dimensions and finger base positions depending on the surface of the grasped object post contact, to give a more stable grasp.

Although the problem of grasp planning has been solved by numerous methods, the formalization of procedures to determine the success of a grasp, as reported by Acuetino-Cabezas *et al.* [29], is not comprehensive. The authors studied and determined conditions that could guarantee the success of a two-dimensional grasp, and hence be able to validate any proposed grasp planning procedure. Similarly, Yan *et al.* [30] used a four-finger tendon-driven robot hand, to demonstrate a method for analyzing the manipulation capabilities of a given prosthetic/robotic hand. Singh and Ambike [31] also presented two metrics: grasp caliber and grasp intensity, to quantitatively decide the stability of a grasp. Dong *et al.* [32] explored the evaluation of grasping quality, by constructing a model of grasp stiffness. This study is also a motivating factor in the development of the contact dynamics model in the present study.

It is to be noted that although there are many algorithms available for minimizing joint torques or calculating optimal contact force distribution during object grasp, most of the studies are typically restricted to hard point contact between rigid bodies [17, 23, 33–36] with few investigations in recent past on soft robotics [37]. However, the investigations reconciling Hertz's contact stress theory with deformable gripper behavior are not comprehensive. Moreover, there are limited studies reporting on the optimal distribution of contact forces and joint torques for a five-fingered, twenty-DoF humanoid robotic hand during object grasp, based on compliant contact (that is, nonlinear spring and damper system), using an energy-based optimization algorithm.

The present study addresses these issues through a novel grasp optimization algorithm, utilizing an energy-based objective function to minimize the net energy required to execute a grasp, taking advantage of redundant DoFs available in a gripper's fingers. The present study also describes a novel approach to instantaneous IK for determining the desirable joint trajectories when multiple contact points are present on the same finger. Hence, to the best of the author's knowledge, the present study of a grasp optimization technique with an objective function derived directly from the theory of compliant grasps, as well as, an IK algorithm to accommodate multiple end effectors on a single serial manipulator has not been attempted before. Although, the optimization algorithm has been developed for a twenty DoF humanoid hand with five fingers (allowing four DoFs in each finger), it can be easily adapted to other types of grippers with redundant DoFs available in their fingers.
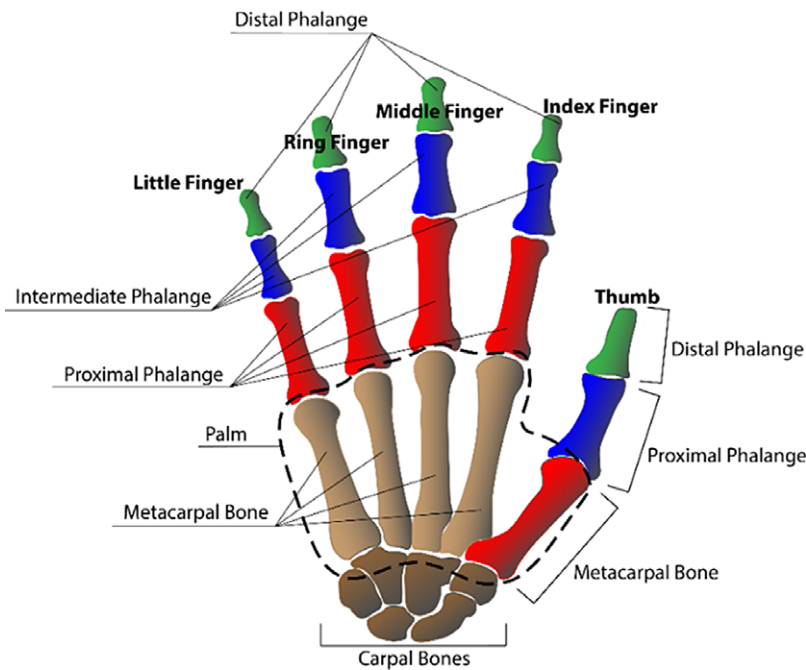
3. Anatomical Description of the Hand

Figure 2 shows the anatomical diagram of the human hand. The robotic humanoid hand gripper used in this study is modeled closely from the anatomical structure of the hand. The index, middle, ring, and little fingers have three movable bones: the proximal, intermediate, and distal phalanges. The proximal phalange of each finger is connected to the palm by a metacarpophalangeal (MCP) joint, which allows two DoFs, one for flexion/extension motion and the other for abduction/adduction motion [38]. The remaining two joints, the proximal interphalangeal (PIP) and distal interphalangeal (DIP) joints, allow one DoF of motion, namely, flexion/extension. In the thumb, the metacarpal bone is connected to the wrist bones (carpal bones) by the carpometacarpal (CMC) joint, which allows two DoFs of motion. The remaining two joints, that is, the MCP and the interphalangeal (IP) joints, allow one DoF of motion, flexion/extension. Thus, each finger has four DoFs of motion, thereby giving a sum total of twenty DoFs for the five-fingered hand. Table I shows the ranges of motion allowed by each joint of each finger, when measured with respect to a fully extended/relaxed position of each finger.

In the present study, a simplified schematic representation of the human hand and fingers with assigned reference frames, kinematic link lengths, and joint angles have been constructed as shown in Fig. 3(a). Figures 3(b) and 3(c) show the generalized schematic diagram of a finger with reference frames assigned. Further, the classical Denavit–Hartenberg (DH) convention [40] has been followed while deriving the kinematic model of the hand. The DH parameters used, for each link of the hand are enlisted in Table II.

The frames are attached at $\mathbb{O}$, $\mathbb{S}_2$, $\mathbb{S}_3$ and $\mathbb{S}_4$ respectively. The base frame {0} is assigned to joint 1 and frame {1} is attached to joint 2, which are co-incident at $\mathbb{O}$. Joint 1 is responsible for

Table I. *Ranges of motion of each joint of the hand (in degrees) [39].*

| Index/Middle/Ring/Little finger			Thumb		
	Flexion-Extension	Abduction-Adduction		Flexion-Extension	Abduction-Adduction
CMC joint	–	–	CMC joint	$-15^0 \sim 90^0$	$0^0 \sim 60^0$
MCP joint	$-40^0 \sim 90^0$	$0^0 \sim (45^0 - 60^0)$	MCP joint	$0^0 \sim 80^0$	–
PIP joint	$0^0 \sim (110^0 - 135^0)$	–	IP joint	$-10^0 \sim 80^0$	–
DIP joint	$-5^0 \sim 90^0$	–	–	–	–

Figure 2. *Anatomical diagram of the human hand.*

abduction/adduction, while joint 2 allows flexion/extension, with link 1 of zero length. Frames {2} and {3} are assigned to joints 3 and 4, respectively, both of which allow flexion–extension motions. Finally, frame {4} is assigned to the tip of the finger. Frame {W} is considered the world reference frame and is attached to the palm. It is to be noted that joints 1 and 2 are separated by a 90^0 twist. The finger phalanges have been simplified as ellipsoids [41]. The dimensions of the ellipsoids' semi-major and semi-minor axes are given in Table III, calculated using anthropometric formulae [42]. The orientations of the semi-major axes are shown in Fig. 3(d). The density of finger phalanges for calculation of its mass is taken as 1160 kg/m [3, 43].

4. Contact Phase Inverse Kinematics

The Contact phase is the most important phase of a grasp, due to its transitional nature. The Contact phase indicates the end of the Approach phase and start of the Grasp phase. The objective is to determine the joint configuration of the finger at the instant of contact, given that the coordinates of the point/points of contact between the finger and the object are known. Generally, IK algorithms deal with a single end effector, reaching a single target coordinate. However, a finger can contact the object at multiple points,
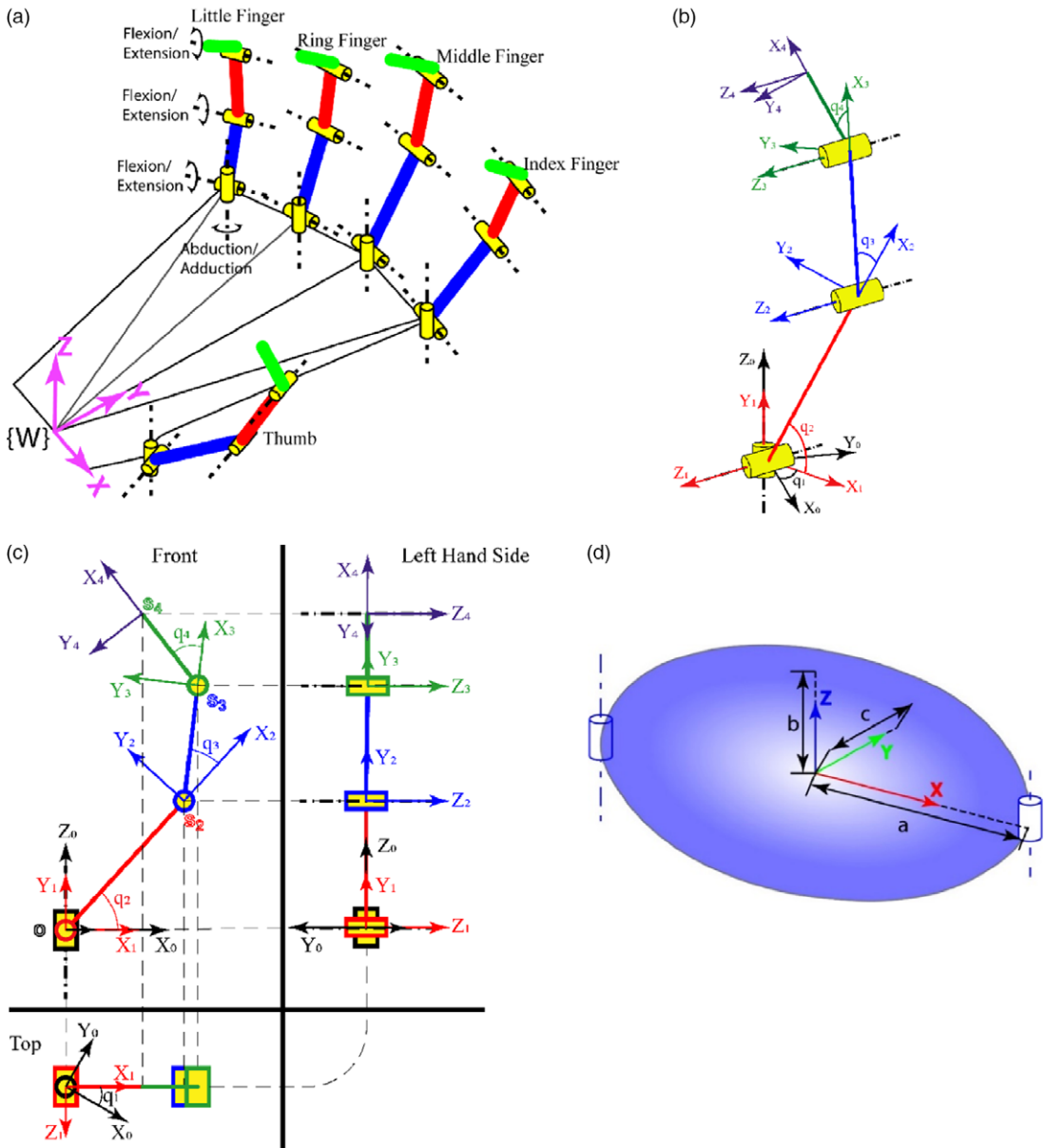
Figure 3. *Schematic representation with reference frames, (a) 20-DoF hand, (b) three-dimensional (3D) view of a finger, (c) two-dimensional (2D) projections of a finger, (d) ellipsoidal geometry of a finger phalange.*

creating multiple target coordinates. The method of IK described in this section uses the sub-manipulator ideology to determine the joint configuration [44–47].

Figure 4 gives an illustration of a finger divided into sub-manipulators, at the time of multiple points of contact between the finger and the object. The advantage of this method lies in the fact that, instead of solving for a finger with L_j contact points, the problem is simplified into solving the IK for L_j sub-manipulators where L_j is the total number of contact points on the jth finger. For this study, there can be a maximum of three contact points between the finger and the object, thus $L_{jmax} = 3$.

Figure 5 shows the various possible contact configurations between any given finger and the object. Figure 5(a) shows a precision grasp, while Figs. 5(b), 5(c) and 5(d) show power grasps [48]. From

Table II. *DH parameters of the five fingered Anthropometric robotic hand.*

| Link	i	q_{ji}	d_i (mm)	l_i (mm)	α_i (deg)
Thumb	1	q_{11}	0	0	90^0
	2	q_{12}	0	55.28	0^0
	3	q_{13}	0	43.16	0^0
	4	q_{14}	0	34.8	0^0
Index Finger	1	q_{21}	0	0	90^0
	2	q_{22}	0	54	0^0
	3	q_{23}	0	31.48	0^0
	4	q_{24}	0	21.36	0^0
Middle Finger	1	q_{31}	0	0	90^0
	2	q_{32}	0	58.58	0^0
	3	q_{33}	0	37.44	0^0
	4	q_{34}	0	23.8	0^0
Ring Finger	1	q_{41}	0	0	90^0
	2	q_{42}	0	53.74	0^0
	3	q_{43}	0	36.34	0^0
	4	q_{44}	0	23.56	0^0
Little Finger	1	q_{51}	0	0	90^0
	2	q_{52}	0	44.92	0^0
	3	q_{53}	0	25.8	0^0
	4	q_{54}	0	20.48	0^0

q_{ji} = Generalized joint coordinate of frame $\{i\}$ with respect to frame $\{i-1\}$ for finger j.
l_i = Length of link i, between the Z_i and Z_{i-1} axes, along the X_{i-1} axis for finger j.
α_i = Angular twist given to link i, measured between Z_i and Z_{i-1} axes, about the X_{i-1} axis for finger j.
d_i = Joint offset given to link i, measured between X_{i-1} and X_i, along the Z_{i-1} axis for finger j.
Here, q_i is the angle of a revolute joint, attached at the base of link i of finger j, measured between X_i and X_{i-1} axes, about the Z_{i-1} axis.

Table III. *Anthropometric dimensions of fingers using ellipsoidal geometry.*

		Digits				
Proximal	Semi major and minor axes	Thumb (mm)	Index finger(mm)	Middle finger(mm)	Ring finger(mm)	Little finger(mm)
1	a	17.40	10.68	11.89	11.78	10.24
	b	7.97	6.83	7.18	6.92	6.30
	c	9.90	8.15	8.23	7.97	7.36
2	a	21.58	15.75	18.72	18.17	12.88
	b	9.37	8.06	8.32	7.80	7.53
	c	9.46	9.02	8.76	8.15	7.62
3	a	27.64	26.98	29.29	26.87	22.46
	b	12.88	9.28	10.00	9.72	8.67
	c	13.14	9.11	8.85	8.50	8.06
4	a	–	50.98	49.11	46.36	45.59
	b	–	17.52	16.03	15.15	14.36
	c	–	21.90	21.90	21.90	21.90
Distal						
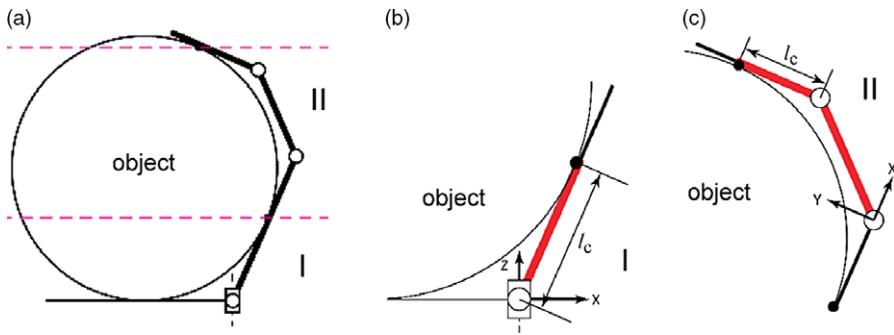
Figure 4. *Illustration to show the division of sub-manipulators, (a) manipulator grasping an object, (b) I: 2-DoFs spatial sub-manipulator, (c) II: 2-DoFs planar sub-manipulator.*
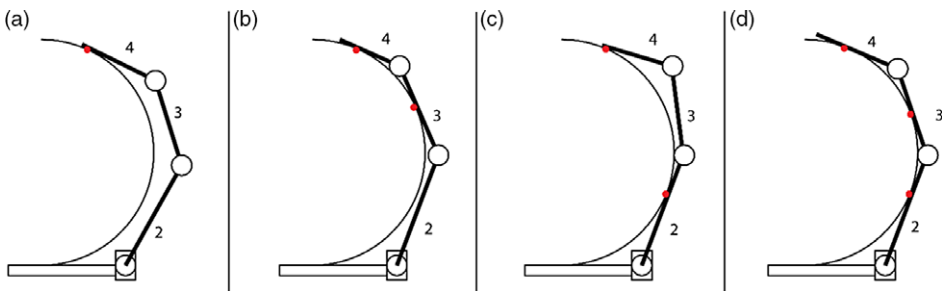
Figure 5. *Various configuration mode of a finger and object during contact, (a) one contact point (4-DoF sub-manipulator with links 2,3,4), (b) two contact points (3-DoF sub-manipulator with links 2, 3 and 1-DoF sub manipulator with link 4), (c) two contact points (2-DoF sub-manipulator with link 2 and 2-DoF sub manipulator with link 3, 4), (d) three contact points (2-DoF sub-manipulator with link 2, 1-DoF sub manipulator with link 3 and 1-DoF sub manipulator with link 4).*
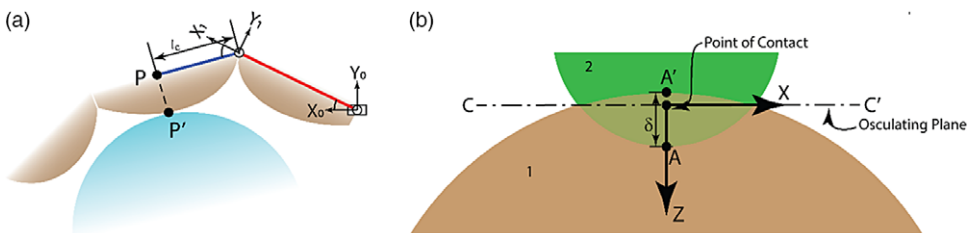

Figure 6. *Schematic representation of, (a) interaction between the finger and object with end-effector point P (in the finger) contacting the object at a point P', (b) interaction between two colliding bodies with the position of the local reference frame.*

Fig. 5, it can be concluded that the finger can form four types of sub-manipulators, depending on the configuration of contact, a 1-DoF sub-manipulator, a 2-DoF sub-manipulator, a 3-DoF sub-manipulator, and a 4-DoF sub-manipulator, which is essentially the entire finger.

Figure 6(a) illustrates the kinematic aspect of the interaction between the finger and the object. The length l_c is termed as the contact length and is used to determine the Jacobian matrix between the point of contact and the base frame of the sub-manipulator [49]. To determine the joint configuration of the complete finger, each sub-manipulator is analyzed one after the other. The solution from the sub-manipulator formed for the first contact point is used to determine the position of the base frame of the next sub-manipulator, and so on. The base point of the first sub-manipulator of any finger will always be the abduction/adduction joint of the finger (CMC joint for the thumb and MCP joint for the rest).
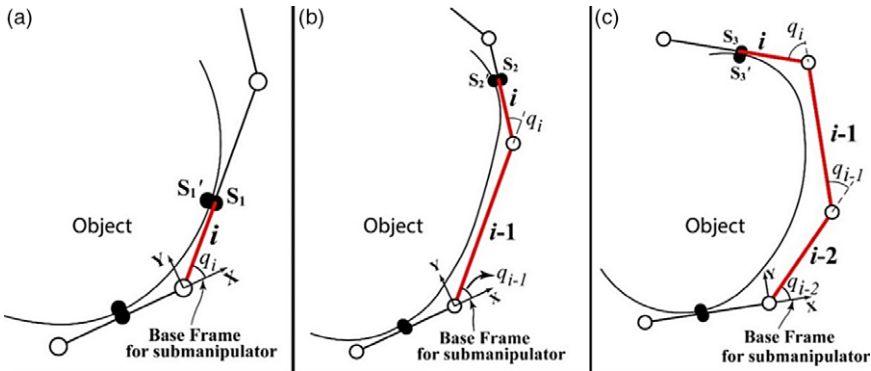
Figure 7. *Illustration of various types of sub-manipulators, (a) 1-DoF sub-manipulator, (b) 2-DoF sub-manipulator, (c) 3-DoF sub-manipulator.*

The joint angle/configuration of the base joint of the first sub-manipulator of any finger can be determined as

$$(q_1)_j = \text{atan2}\left(\{y_P\}_0, \{x_P\}_0\right), \tag{1}$$

where $(q_1)_j$ is the abduction/adduction (or the base joint) angle of the jth finger, $\{x_P\}_0$ and $\{y_P\}_0$ are the x and y coordinates of the first contact point 'P' measured with respect to frame $\{0\}$ (or the base frame) of the finger. Fixing the abduction/adduction angle (joint angle of the base joint) fixes the flexion/extension plane as well. Hence, once the base joint angle is calculated using Eq. (1), all the sub-manipulators can be treated as planar in nature. As a result, the IK of the first sub-manipulator can be solved by simply reducing its initial DoFs by 1. The end of the link contacting the object is assumed to be the base for the next consecutive sub-manipulator.

Figure 7(a) shows the general depiction of a 1-DoF sub-manipulator followed by a 2-DoF sub-manipulator shown in Fig. 7(b) and a 3-DoF sub-manipulator shown in Fig. 7(c). Only planar cases have been considered, due to the reasons mentioned above. Based on Fig. 7(a), the joint angle for a 1-DoF sub-manipulator can be easily calculated as

$$(q_i)_j = \text{atan2}\left(\left\{y_{S_1'}\right\}_{i-1}, \left\{x_{S_1'}\right\}_{i-1}\right), \tag{2}$$

where $(q_i)_j$ is the ith joint angle of the sub-manipulator of the jth finger; $\left\{x_{S_1'}\right\}_{i-1}$ and $\left\{y_{S_1'}\right\}_{i-1}$ are the x and y coordinates of the contact point S_1' for the 1-DoF manipulator, measured in the frame $\{i-1\}$. Here, link/joint number i refers to the end-effector link of the sub-manipulator. The preceding links are numbered as $i-1$ and $i-2$, as shown in Figs. 7(b) and 7(c).

Similarly, the joint angles for a 2-Dof sub-manipulator (refer to Fig. 7(b)) are given by

$$(q_{i-1})_j = \text{asin}\left(\frac{l_{i-1}^2 - l_c^2 + \left\{x_{S_2'}\right\}_{i-2}^2 + \left\{y_{S_2'}\right\}_{i-2}^2}{2l_{i-1}\sqrt{\left\{x_{S_2'}\right\}_{i-2}^2 + \left\{y_{S_2'}\right\}_{i-2}^2}}\right) - \text{atan2}\left(\left\{x_{S_2'}\right\}_{i-2}, \left\{y_{S_2'}\right\}_{i-2}\right), \tag{3a}$$

$$(q_i)_j = \text{asin}\left(\frac{\left\{y_{S_2'}\right\}_{i-2}\cos(q_{i-1}) - \left\{x_{S_2'}\right\}_{i-2}\sin(q_{i-1})}{l_i}\right), \tag{3b}$$

where q_i and q_{i-1} are the joint angles of the 2-DoF sub-manipulator and l_i is the length of the ith link. The contact length l_c can be determined from the MSC.Adams® simulation.

Again, for a 3-DoF planar sub-manipulator, the redundant DoF does not allow for a closed-form solution. Hence, the possible solutions are determined by fixing the base joint angle and solving the IK

problem for the remaining two links as a 2-DoF sub-manipulator (refer to Eqs. (3a) and (3b)). Multiple such base-joint angles are considered between an interval of $\pm 3°$, based on the original Contact phase configuration determined from the MSC.Adams® simulation.

5. Grasp-Energy-based Optimization

5.1. Hand and object interaction modeling

As previously mentioned, the contact dynamics in this study follows the Hertzian contact stress theory. The normal force on contact, F_n, is calculated using a modified Hunt and Crossley non-linear spring-damper model presented by Marhefka and Orin [3, 50] and is given by

$$F_n = (\lambda \delta^\rho)\,\dot\delta + K\delta^\rho, \tag{4}$$

where K is the contact stiffness; λ is the damping co-efficient; δ gives the penetration depth, that is, the total distance between A and A′ as shown in Fig. 6(b); $\dot\delta$ gives the relative penetration velocity of body 1 with respect to body 2, along the local contact frame $\hat{Z}$-axis and ρ is the contact exponent. In the present study, ρ is set equal to 1.5, assuming nonconforming contacts [3, 51].

Also, assuming no-slip conditions, the friction force along each axis is calculated as

$$f_x, f_y \le |\mu F_n|, \tag{5}$$

where f_x is the friction force along the $\hat{X}$-axis and f_y is the friction force along the $\hat{Y}$-axis. It is to be noted that Eqs. (4) and (5) have been represented in a local frame of reference, placed at the point of contact, as shown in Fig. 6(b). Normal force at contact, F_n, points along the $+\hat{Z}$-axis of the local reference frame, that is, into the object 1. The X-Y plane lies parallel to the osculating plane CC′ containing the point of contact, and the $\hat{Z}$-axis is directed toward the object and lies along the normal to the contacting surfaces or osculating plane at the point of contact. Assuming that the torque acting at the point of contact is negligible, the force-torque wrench vector in the local frame of the ith contact point can be defined as

$$(h_e)_i = \left(f_x, f_y, F_n\right)^T, \tag{6}$$

and the vector $(h_e)_i$ can be transformed [52] to a new frame $\{k\}$ as

$$(h_e)_k = {}^i_k R^*(h_e)_i, \tag{7}$$

where ${}^i_k R$ is the rotational transform of frame $\{k\}$ with respect to frame $\{i\}$.

5.2. Objective function

Successful execution of a grasp depends on the invariance of the object coordinates within its configuration space [29]. The grasps described in this study assume force-closure conditions, to ensure stable grasps [53, 54]. Using this concept as the primary constraint, and the fact that the contact mechanics has been modeled using the principles of compliant contact between objects, an energy-based optimization performance measure has been formulated, and termed as Grasp-Energy.

The objective function has been derived using the principles of virtual work. In static friction conditions, penetration progressess only along the $\hat{Z}$-axis of the local contact-point coordinate frame. Hence, the instantaneous work done (dW) can be written as

$$dW = F_n \cdot d\delta + dF_n \cdot \delta. \tag{8}$$

As the work done at any instant during collision depends on the amount of penetration, then for an incremental change in penetration depth, dδ the work done will be

$$\frac{dW}{d\delta} = F_n + \frac{dF_n}{d\delta}\delta. \tag{9}$$

Substituting Eq. (4) in Eq. (9) and differentiating the expression reduces to

$$\frac{\mathrm{d}W}{\mathrm{d}\delta} = (\rho + 1)\left(\lambda\dot{\delta} + K\right)\delta^{\rho}. \tag{10}$$

The net work done or the net energy consumed, between the time of impact t_I and time of completion of grasp t_F, can thus be obtained as

$$GE_{ji} = \int_{t=t_I}^{t_F} (\rho + 1)\left(\lambda\dot{\delta} + K\right)\delta^{\rho}\mathrm{d}t, \tag{11}$$

where GE_{ji} represents the Grasp-Energy required at the ith contact point of the jth finger.

The total Grasp Energy of the hand can be summed numerically across all contact points of all fingers and is given by

$$GE = \sum_{j=1}^{N}\sum_{i=1}^{L_j} GE_{ji} \tag{12}$$

Here, N gives the total number of fingers contacting the object and L_j gives the total number of points of contact on the jth finger. Therefore, minimizing Eq. (12) subject to equality and inequality constraints is the objective of the optimization problem.

5.3. Constraint Definitions

The derivation and subsequent optimization of the objective function is subject to certain assumptions:

1. The surface of the object being grasped is convex, that is, facing away from the center of the object at the points of contact.
2. The surface of the object is continuous and differentiable at the point of contact.
3. The links of the fingers that collide with the object, do so simultaneously at the same time of impact.

Now, based on the above assumptions, the following constraints are applied on the objective function:

a) *Geometric constraints*: The geometric constraints define the bounds of the design variables δ, $\dot{\delta}$ and instantaneous penetration acceleration $\ddot{\delta}$ and is given by

$$0 \le \delta \le \delta_{max}, \tag{13a}$$

$$0 \le \dot{\delta} \le \dot{\delta}_I \le \dot{\delta}_{max}, \tag{13b}$$

$$-\left|\ddot{\delta}_{max}\right| \le \ddot{\delta} < 0, \tag{13c}$$

where δ_{max} gives the maximum allowable penetration depth, based on the object's and fingers' mechanical properties; $\dot{\delta}_I$ is the velocity of link at impact; $\dot{\delta}_{max}$ gives the maximum allowable penetration velocity based on the allowable joint actuation velocities, and $\left|\ddot{\delta}_{max}\right|$ gives the magnitude of the maximum allowable penetration acceleration, depending on the capabilities of the actuators used. The penetration acceleration must always be negative, once the fingers come into contact with the object, in order to decelerate the fingers after impact.

b) *Allowable time of impact*: The bounds on the allowable times of impact are set by this constraint, such that
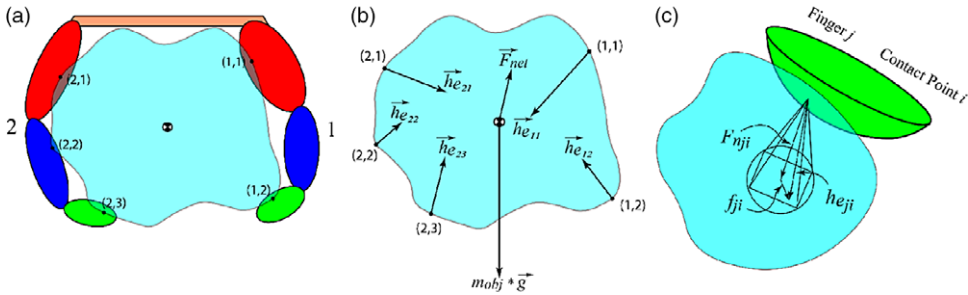
Figure 8. *Schematic representation, (a) fingers 1 and 2 grasping an object, (b) free-body diagram of the object with forces acting on it during grasp, (c) friction pyramid constraint and friction forces during interaction at the ith contact point of the jth finger with a rigid object.*

$$0 < t_{I_{min}} \leq t_I \leq t_{I_{max}} < t_F. \tag{14}$$

where $t_{I_{min}}$ gives the minimum allowable time of impact, $t_{I_{max}}$ gives the maximum allowable time of impact, t_F is the pre-set time of completion of grasp, and t_I is the selected time of impact for optimization. It is to be noted that at $t = t_F$, the generated net contact force vector is intended to create static equilibrium conditions for the object being grasped.

c) *Static equilibrium equation*: The static equilibrium constraint fulfills the condition of invariance of object coordinates, by constraining the optimal solution set to maintain the object's static equilibrium, at the end of the grasp (refer to Fig. 8).

The static equilibrium equation is given by

$$\left\{ \sum_{j=1}^{N} \sum_{i=1}^{L_j} \vec{h}_{e_{ji}} \right\}_{t=t_F} + \vec{F}_e = 0. \tag{15}$$

where $\vec{h}_{e_{ji}}$ is the vector of net contact force acting on the object at the ith contact point (corresponding to the ith link in contact) of the jth finger ; $\vec{F}_e$ is the sum of all external force vectors acting on the object. Further, Eq. (15) implies that complete static equilibrium can be achieved only at the time of completion of grasp. It is to be noted that the constraints are set, such that minimum energy is required to precisely grasp the object. Hence, the reaction force of the palm on the object has been neglected in this study (refer to Fig. 8(b)) since its effect is predominant when more force is required to neutralize all the external forces.

d) *Friction force constraints*: The static friction force constraints govern the selection of the force vector. The friction cone constraints generally used in such situations [4, 54] can instead be reduced to a much more conservative set of linear constraints for a friction pyramid (refer to Fig. 8(c)) expressed as

$$-f_{ji}^x + \frac{\mu}{\sqrt{2}} F_{n_{ji}} < 0, \tag{16a}$$

$$f_{ji}^x + \frac{\mu}{\sqrt{2}} F_{n_{ji}} < 0, \tag{16b}$$

$$-f_{ji}^y + \frac{\mu}{\sqrt{2}} F_{n_{ji}} < 0, \tag{16c}$$

$$f_{ji}^{y} + \frac{\mu}{\sqrt{2}}F_{n_{ji}} < 0, \tag{16d}$$

where f_{ji}^{x} is the force of friction along the X-axis of the local coordinate frame at the point of contact of the ith link of the jth finger, f_{ji}^{y} is the force of friction along the Y-axis of the local coordinate frame at the point of contact at the ith contact point (corresponding to the ith link in contact) of the jth finger, and μ is the coefficient of friction that is assumed to be uniform for all contact points.

6. Approach and Grasp Phase Trajectory Generation

6.1. Grasp phase

The possible Grasp phase joint trajectories are calculated taking into consideration both the multiple Contact phase IK solutions as well as the impact penetration velocity and acceleration values determined using the optimization algorithm. Thereafter, the set of Grasp phase joint trajectories that utilizes the least joint torque norm can then be used for determining the Approach phase joint trajectories.

Computation of the optimal values of penetration accelerations for each finger and impact time leads to the determination of the joint trajectory of the fingers for the Grasp phase. Due to the nature of the optimization algorithm, each link contacting the object is assigned an optimal penetration depth, impact velocity, and impact acceleration values. Thus, each sub-manipulator needs to follow the cartesian trajectory assigned to its end effector to achieve an optimal grasp. For this, an algorithm has been developed that uses the method of instantaneous IK for each sub-manipulator, to iteratively calculate the joint configuration of the finger. Assuming that the inverse kinematic solution for a given set of trajectories for a finger exists, the following equations can be used to iteratively calculate the desired joint trajectories, for each sub-manipulator, at a given time step:

1. For the first sub-manipulator with m DoFs (including the DoF of the abduction/adduction joint), the joint velocity vector is given by

$$\begin{pmatrix} \dot{q}_1 \\ \vdots \\ \dot{q}_i \end{pmatrix}_{m \times 1} = \left({}^{0}J_i\right)^{\#}_{i \times 3} {}^{*}\left({}^{0}V_i\right)_{3 \times 1}. \tag{17a}$$

2. For each subsequent sub-manipulator, the equation to be used is given by

$$\begin{pmatrix} \dot{q}_{i+1} \\ \vdots \\ \dot{q}_k \end{pmatrix}_{(k-i) \times 1} = \left({}^{0}J_k\right)^{\#}_{(i+1:k) \times 3} \left[\left({}^{0}V_k\right)_{3 \times 1} - \left({}^{0}J_k\right)_{(1:m) \times 3} \begin{pmatrix} \dot{q}_1 \\ \vdots \\ \dot{q}_i \end{pmatrix}_{i \times 1} \right], \tag{17b}$$

where $\dot{q}_i$ is the joint velocity of the ith joint, ${}^{0}J_k$ is defined as the jacobian matrix for the kth contact point with respect to the base frame of that finger [49], ${}^{0}J_k^{\#}$ represents the Damped-Least-Square (DLS) inverse of the Jacobian [55] for the kth contact point, and ${}^{0}V_k$ is the target velocity of the kth contact point. It is also to be noted that, in the present case $\left({}^{0}J_k\right)_{(a1:a2) \times b}$ specifies a submatrix of ${}^{0}J_k$, consisting of rows a_1 to a_2 and b columns.

Now, using Eqs. (17a) and (17b), the joint velocities at a given time step for a finger are calculated iteratively. The desired joint configuration for the current time step is thus updated and given by

$$q_{current} = q_{previous} + \dot{q}_{current}{}^{*}\Delta t \tag{18}$$

Likewise, the desired motion of all the fingers can be calculated iteratively. Thereafter, the Contact phase configuration with the minimum Grasp phase torque norm is then selected to determine the Approach phase joint trajectory. The joint torques are determined using the dynamic equations of motion [40, 56].
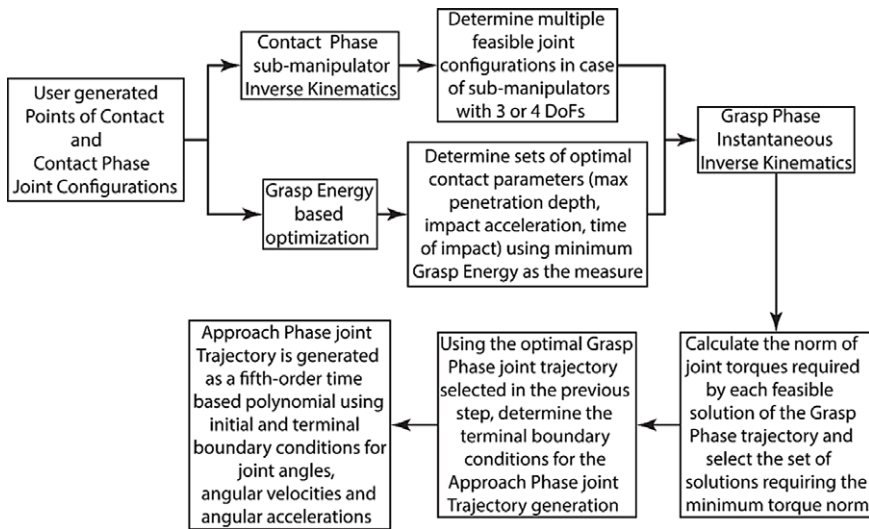
Figure 9. *Block diagram showing various stages of the grasp optimization algorithm.*

6.2. Approach phase

Using the boundary conditions at the optimal initial time of impact, t_I^*, along with the Grasp phase joint trajectories' values, the Approach phase joint trajectories can be easily determined as a time-based polynomial function of fifth order given by

$$q_{ij} = a_0 + a_1 t + a_2 t^2 + a_3 t^3 + a_4 t^4 + a_5 t^5 \tag{19}$$

The necessary boundary conditions for determination of the coefficients of the polynomial function during Approach phase are given by

(i) $t = 0$, $q_{ij} = 0$, $\dot{q}_{ij} = 0$, $\ddot{q}_{ij} = -\ddot{q}_{ij}^*$, at

(ii) at $t = t_I^*$, $q_{ij} = q_{ij}^*$, $\dot{q}_{ij} = \dot{q}_{ij}^*$, $\ddot{q}_{ij} = \ddot{q}_{ij}^*$.

The step-wise working of the entire grasp algorithm has been explained in the Appendix.

7. Numerical Illustration

The block diagram shown in Fig. 9 demonstrates the working of the grasp optimization algorithm. After the object has been grasped, interaction forces generated between the object and the fingers at the points of contact (termed as contact forces) are determined, before computation of the joint torques required to secure the grasp. However, it is to be noted that the approach is computationally intensive and carried out offline with the predefined boundary conditions for the determination of a set of optimal force-space configurations.

To demonstrate the efficacy of the developed grasp optimization algorithm, computer simulations are run in MATLAB® and compared with simulations using Virtual Prototyping (VP) tools, like the commercially available numerical solver MSC.Adams®. The coordinates of the points of contact and a desired joint configuration at the Contact phase are required to be given as initial input (refer to Section 6), which are obtained from the simulation model (refer to Fig. 10) in MSC.Adams®, with the same boundary conditions. The world reference frame {W} with $X_w Y_w Z_w$ axes system is fixed at the bottom of the object, as shown in Fig. 10. The subscript 'bj' is used to indicate the axes of the base frame of the jth finger. Gravity acts, along the axis of the cylinder, in the $-Z_w$ direction.

Table IV. *Input joint trajectory ranges assigned to the hand in MSC.Adams®
Simulation.*

| Finger	Joint	Joint Trajectory
Thumb	CMC Joint (Ab/Add)	$0° \sim 130°$
	CMC Joint (Fl/Ext)	$0° \sim 72°$
	MCP Joint	$0° \sim 50°$
	IP Joint	$0° \sim 30°$
Index Finger	MCP Joint (Ab/Add)	$0° \sim 10°$
	MCP Joint (Fl/Ext)	$0° \sim 82°$
	PIP Joint	$0° \sim 30°$
	DIP Joint	$0° \sim 30°$
Middle Finger	MCP Joint (Ab/Add)	$0° \sim 0°$
	MCP Joint (Fl/Ext)	$0° \sim 71°$
	PIP Joint	$0° \sim 50°$
	DIP Joint	$0° \sim 30°$
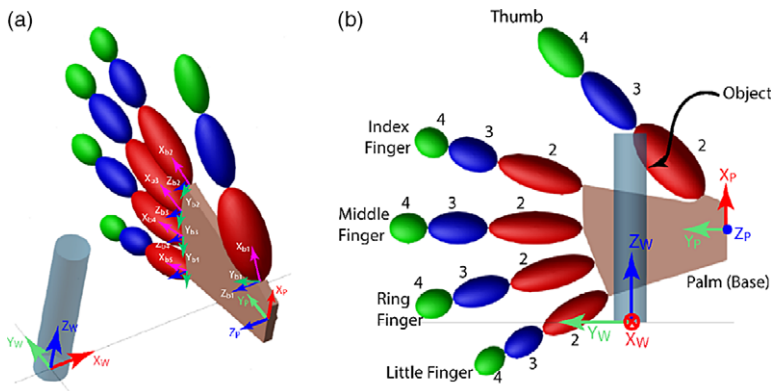
Figure 10. *Reference frames and initial configuration of the robot hand model for precise grasping of a small cylindrical object, (a) Isometric view, (b) Front view.*

In the MSC.Adams® simulation, the object to be grasped is treated as a ground object to fulfill the invariance condition. Predefined joint trajectories are provided to each joint of the three fingers, namely, thumb, index, and middle, as given in Table IV. These grasp trajectories are generated using trial and error method to imitate a user's action, before it is optimized and passed on to the actual robotic gripper. The coordinates of the points of contact between the gripper and object, obtained from the dynamic simulation in MSC.Adams®, are exported to MATLAB, where a numerical simulation of the algorithm is run, using the same boundary conditions.

The values of the common boundary conditions chosen for the simulation are given in Table V. In order to determine the desired force-space configuration, a direct grid-search method is adopted, wherein the possible force combinations amongst all contact points are evaluated, to test whether a configuration satisfies all constraints. Due to the limitation of using a grid-search algorithm, the possible forces within the force pyramid of each contact point are discretized. As a result of the discretization of forces, it is difficult to obtain a force-space configuration that can completely balance out the external forces acting on the object. Hence, in order to satisfy the equilibrium constraint, a maximum limit on the allowable net force (the sum of all contact forces and external forces) is set for the case study. Any force-space configuration whose sum of the external forces lay below the allowable limit is selected to check if the vectors further satisfied the remaining constraints. Due to this, the total number of contact points

Table V. *Common input parameters for the case study.*

| Parameter	Magnitude
Simulation End Time (t_F)	1 sec
$t_{I_{min}}$	0.8 sec
$t_{I_{max}}$	0.95 sec
$\ddot{\delta}_{min}$	0.01 m/s^2
$\ddot{\delta}_{max}$	1 m/s^2
$\dot{\delta}_{max}$	2 m/s
δ_{max}	5 mm
Axis of gravitational acceleration	-Z_W
K	50 N/mm
λ	0.1 N/mm-s
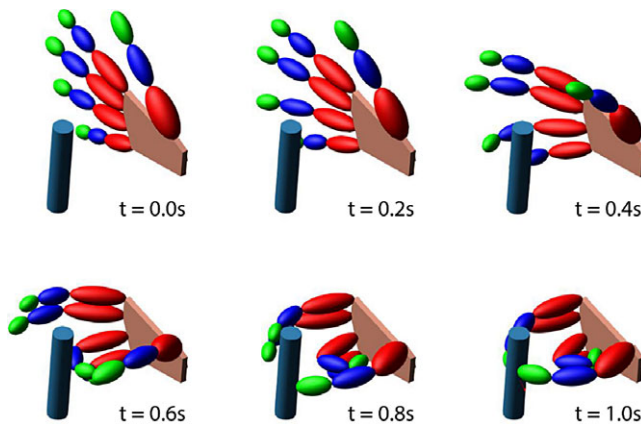
Figure 11. *Snapshots of the robot hand motion for grasping a small object (cylinder) simulated in MSC.Adams®.*

between the hand and the object has been restricted to three, that is, a precision grasp is chosen for the demonstration. The hand motion is simulated to grasp a solid cylinder (similar to grasping a pen/pencil's stem), with three fingers, namely, the thumb, the index finger, and the middle finger as mentioned in Table IV. However, it is to be noted that the angular displacement of the CMC joint (abduction/adduction joint) of the thumb (approximately, 130°) is large and has been provided as input to the joint trajectory in MSC.Adams® simulation (refer to Table IV). This angle is beyond the ranges of motion described for a human hand in Table I, and therefore, it perfectly encompasses the limitations of a simplified humanoid hand model.

The actual human hand is a complex structure, and a robotic model of the hand can only imitate the human in an approximate manner. Hence, such a large abduction/adduction motion has been assigned to the thumb since it is necessary for the proper execution of its opposition motion in the constraints of the developed model. Snapshots of the hand motion sequence at regular intervals of the simulation are shown in Fig. 11.

At the end of simulation, three points of contact are obtained, as shown in Fig. 12. Since the object is grasped with the tips of each finger, three 4-DoF sub-manipulators are formed. Using the IK algorithm described in Section 4, the first joint angle is calculated, thereby reducing the problem into a 3-DoF planar sub-manipulator whose base angle is the second joint of the finger. The angle base joint of the 3-DoF sub-manipulator is fixed at various points within ±3° of the initial configuration at contact, and the IK solution for the remaining two links is determined for each value of the base joint angle. The set
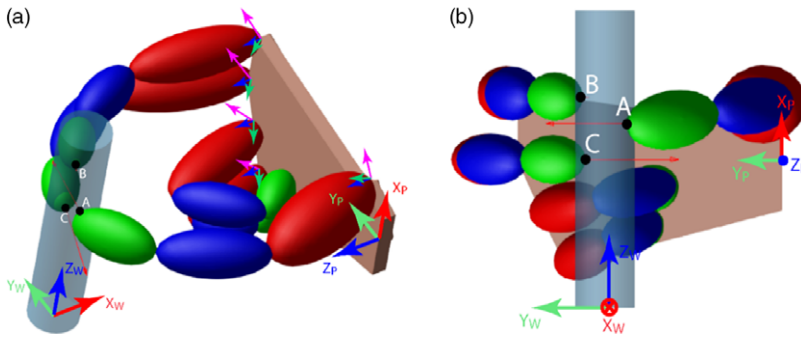
Figure 12. *Position of the robot hand model and location of the three points of contact after completion of grasp (at t = 1.0s), (a) Isometric view, (b) Front view. The ring finger and little finger follow independent joint trajectories, to make it look similar to an actual precision grasp.*
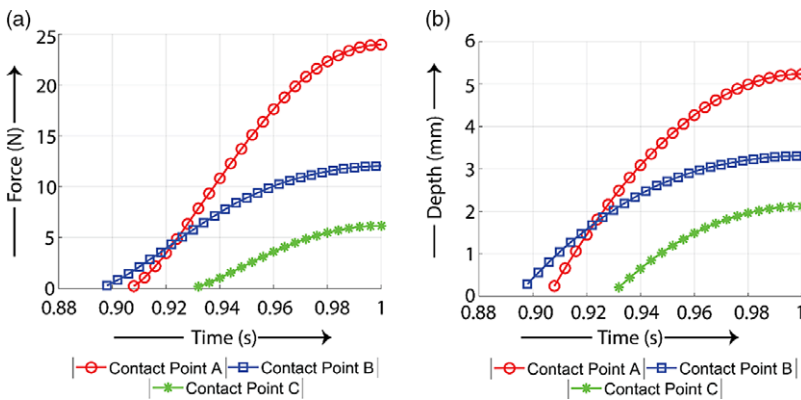

Figure 13. *Simulated data of the points of contact in MSC.Adams®, (a) the normal force distribution, (b) the penetration depth profile.*

of contact points (C_P) obtained from the MSC.Adams® simulation (dimensions are in millimeters) is given by

$$C_P = \begin{pmatrix} x_A & x_B & x_C \\ y_A & y_B & y_C \\ z_A & z_B & z_C \end{pmatrix}_W = \begin{pmatrix} -2.6 & 4.7 & 1.7 \\ -9.6 & 8.8 & 9.7 \\ 61.5 & 71.0 & 50.0 \end{pmatrix}$$

The total Grasp Energy is calculated as 73.6 N-mm using the simulated data from MSC.Adams® as shown in Fig 13. The boundary conditions, Contact phase joint configurations, and coordinates of points of contact obtained from MSC.Adams® simulation are provided as input to the analytical model simulated in MATLAB. The cartesian coordinates of the points of contact and the possible joint configurations at the Contact phase are supplied as input to the optimization algorithm run in MATLAB. The output data are post processed, and the trajectory with the minimum net Grasp Energy is selected, which has a value of 55.9 N-mm.

Figure 14 compares the joint trajectory data (angular displacement) of the hand model simulated in MSC.Adams® with that of the analytical data obtained using the optimization algorithm simulated in MATLAB. Figures 14(a), 14(b) and 14(c) show the angular displacement of the joints of the thumb, index finger, and middle finger, respectively, obtained from the MSC.Adams® simulation, whereas Figs. 14(d), 14(e) and 14(f) give the angular displacement of the above-mentioned joints computed using the optimization algorithm with indication of the Approach and the Grasp phases. It is seen that
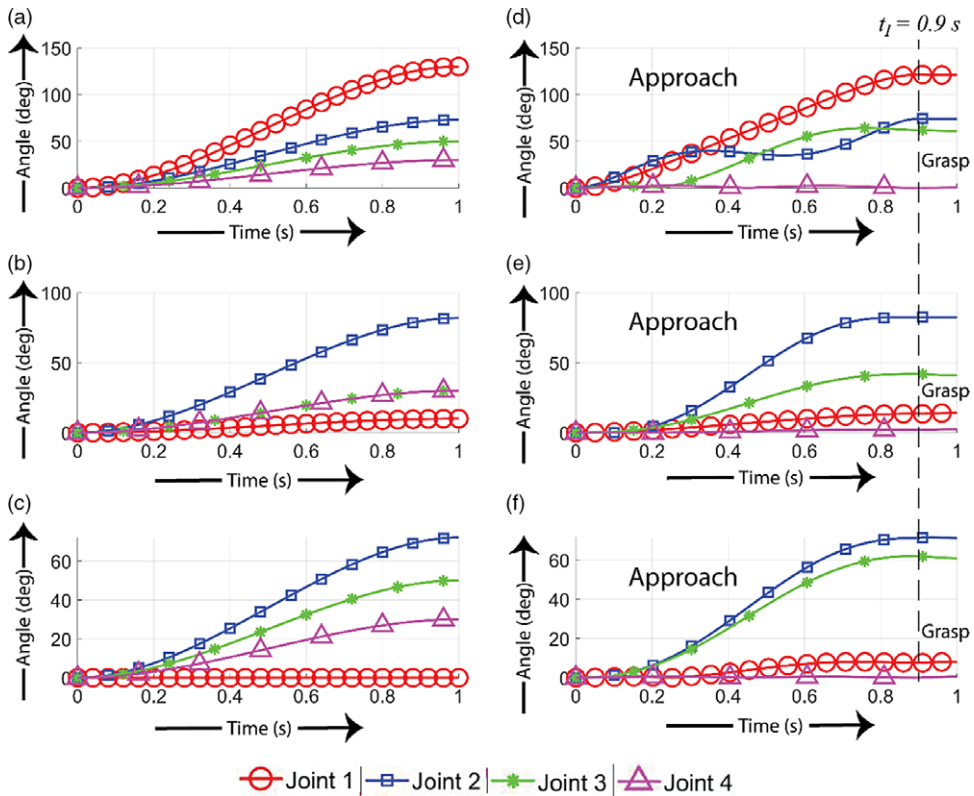
Figure 14. *Joint trajectory profiles of the robot hand when grasping a cylindrical object in the CAD simulation for (a) the Thumb, (b) the Index finger, (c) the Middle finger, and using results from the Optimization algorithm for (d) the Thumb, (e) the Index finger, (f) the Middle finger.*

the optimal time of impact, selected by the algorithm is $t_I = 0.9$ s. For $t > t_I$, the joint trajectories are calculated using the Grasp phase IK algorithm given in Section 6.1.

Figure 15 gives a comparison of the joint torque distribution of the thumb obtained from MSC.Adams® (Fig. 15(a)) simulation with that of the optimal joint torque distribution (analytical) computed in MATLAB (Fig. 15(b)). The graphical plot during Approach phase shows the joint torque distribution before contact between the object and the thumb, while the plot during Grasp phase shows the joint torque distribution after contact has been established. It is observed that the maximum torque lies in the range $1.5 \times 10^{-2} \sim 2.0 \times 10^{-2}$ N-m during the Approach phase and within $0.3 \sim 0.4$ N-m during the Grasp phase in both the cases, that is, MSC.Adams® and the Analytical solution computed in MATLAB. The maximum torque in the Approach phase for the MSC.Adams® simulation before optimization is 1.81×10^{-2} N-m for joint 1, 1.37×10^{-2} N-m for joint 2, 4.8×10^{-3} N-m for joint 3, and 9.5×10^{-4} N-m for joint 4. The corresponding maximum joint torques in the Approach phase for the MATLAB simulation are 1.84×10^{-2} N-m for joint 1, 1.47×10^{-2} N-m for joint 2, 5×10^{-3} N-m for joint 3, and 9.6×10^{-4} N-m for joint 4. For the Grasp phase, the maximum joint torques in the MSC.Adams® simulation are 2.7×10^{-2} N-m for joint 1, 0.34 N-m for joint 2, 0.19 N-m for joint 3, and 6.2×10^{-2} N-m for joint 4, while the torques required after optimization are 9.1×10^{-3} N-m for joint 1, 0.31 N-m for joint 2, 0.18 N-m for joint 3, and 6.95×10^{-2} N-m for joint 4. As a consequence of optimization, the maximum joint torques required after contact are noticeably lower compared to the torques required prior to implementation of the optimization algorithm.

Similarly, a comparative study of the joint torque distribution of the index finger obtained from MSC.Adams® and analytical solution in MATLAB are also investigated as shown in Figs. 16(a) and 16(b), respectively. The joint torque requirement of the index finger is below 1×10^{-2} N-m for the
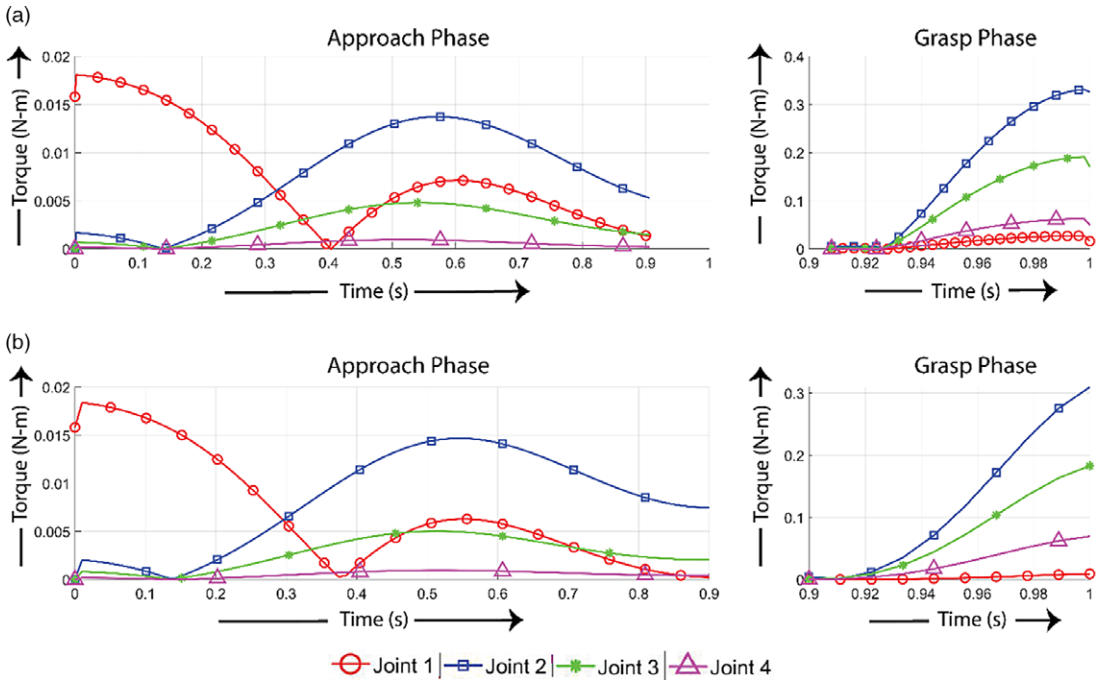
Figure 15. *Torque distribution in various joints of the thumb, (a) Simulated data in MSC.Adams®, (b) Analytical data using optimization algorithm.*
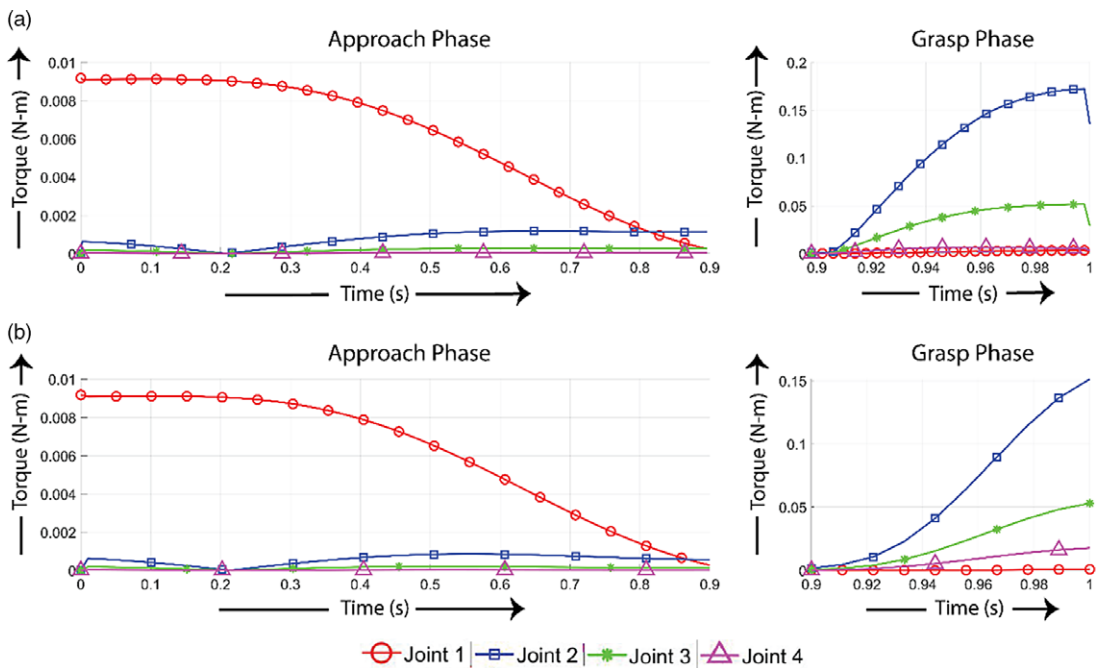

Figure 16. *Torque distribution in various joints of the index finger, (a) Simulated data in MSC.Adams®, (b) Analytical data using optimization algorithm.*
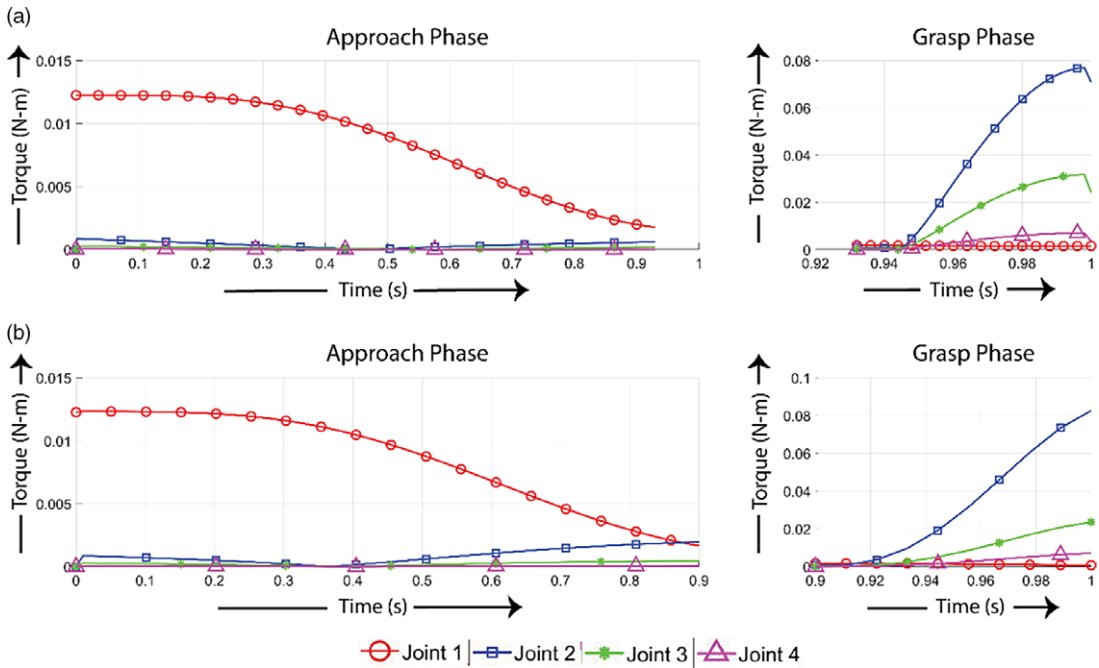
Figure 17. *Torque distribution in various joints of the middle finger, (a) Simulated data in MSC.Adams®, (b) Analytical data using optimization algorithm.*

Approach phase and increases to $0.15 \sim 0.2$ N-m for the Grasp phase. The maximum joint torques registered in the Approach phase is about 9.1×10^{-3} N-m for joint 1, 1.1×10^{-3} N-m for joint 2, 2.8×10^{-4} N-m for joint 3, and 3.8×10^{-5} N-m for joint 4 before optimization, while the maximum torques after optimization are 9.1×10^{-3} N-m for joint 1, 8.5×10^{-4} N-m for joint 2, 2×10^{-4} N-m for joint 3, and 2.95×10^{-5} N-m for joint 4. The maximum joint torques registered in the Grasp phase is 3.3×10^{-3} N-m for joint 1, 0.172 N-m for joint 2, 5.1×10^{-2} N-m for joint 3, and 6.5×10^{-3} N-m for joint 4 in the MSC.Adams® simulation (before optimization), while the values after optimization reduce down to 8.4×10^{-4} N-m for joint 1, 0.15 N-m for joint 2, 5.3×10^{-2} N-m for joint 3, and 1.7×10^{-2} N-m for joint 4 in the MATLAB simulation, after optimization. In comparison to that of the thumb, the joint torque requirements for the index finger are significantly reduced. First, this may be attributed to the lower mass of the finger, compared to the thumb (mass of the index finger is approximately 20 g based on the anthropometric values chosen in this study, while the mass of the thumb is close to double that, approximately 39 g). Second, it is due to the overall joint angle displacement of each finger, the net joint displacements of the thumb are larger than those of the joints of the index finger, as seen from Fig. 14. Due to these reasons, the torque requirements for the joints increase significantly.

Finally, Figs. 17(a) and 17(b) shows the comparative results of the joint torque distribution for the motion of the middle finger both obtained from numerical simulation in MSC.Adams® and analytical data using optimization. The joint torque requirement of the middle finger lies below 1.5×10^{-2} N-m for the Approach phase and increases to $8 \times 10^{-2} \sim 0.1$ N-m for the Grasp phase. The maximum joint torques computed in the Approach phase is about 1.23×10^{-2} N-m for joint 1, 8.53×10^{-4} N-m for joint 2, 2.77×10^{-4} N-m for joint 3, and 4.65×10^{-5} N-m for joint 4 before optimization, while the maximum torques after optimization are 1.23×10^{-3} N-m for joint 1, 1.96×10^{-3} N-m for joint 2, 4.5×10^{-4} N-m for joint 3, and 6.86×10^{-5} N-m for joint 4. The maximum joint torques registered for the middle finger in the Grasp phase is 1.5×10^{-3} N-m for joint 1, 7.7×10^{-2} N-m for joint 2, 3.18×10^{-2} N-m for joint 3, and 7×10^{-3} N-m for joint 4 in the MSC.Adams® simulation (before optimization) while the values after optimization change to 7.7×10^{-4} N-m for joint 1, 8.25×10^{-2} N-m for joint 2, 2.36×10^{-2} N-m for joint 3, and 7.18×10^{-3} N-m for joint 4 in the MATLAB simulation, after optimization. For all three
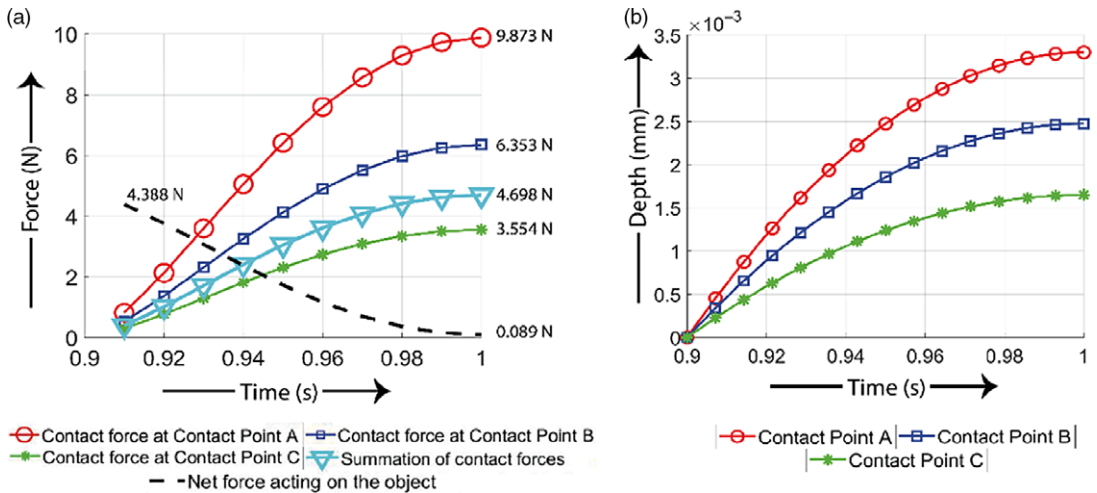
Figure 18. *(a) Normal Contact force distribution , (b) penetration depth profiles for the optimized motion of the hand in the Grasp phase.*

fingers, joint 1 has the maximum torque load. This is mainly due to the fact that the gravitational axis points in the $-Z_W$ direction in the simulation. The torque generated by the weight of each phalange on joint 1 directly opposes the torque required to hold the fingers stable. In the Grasp phase, after the finger contacts the object, the torque required to counter the finger weight is instead provided by the friction force acting at the tip, thus reducing the load on the abduction/adduction joint and leaving the flexion/extension joints to deal with the contact stress generated.

Both the normal contact force distribution at each point of contact between the finger and the object and the net force acting on the object due to the fingers are shown in Fig. 18(a). Here, the normal contact forces shown are calculated with respect to the reference frame placed at the point of contact, described in Fig. 6(b). At the start of the Grasp phase, the net force acting on the object is zero, corresponding to zero penetration depth. Now, as the penetration depth increases, the net force on the object increases accordingly and succeeds in nearly countering the other external forces acting on it. Figure 18(b) shows the penetration depth profiles between the fingers and object at each point of contact. Further, it is to be noted that in this study, only gravitational force has been considered as an external force. There is a residual force of ~0.089 N acting on the object at the end of the grasp, for a given set of contact forces and contact friction forces. The thumb provides the opposition motion, and hence exerts the maximum contact force of 9.873 N in order to counter the forces exerted by the other two fingers. Since the location of contact points is random, the contact forces exerted by the index and middle fingers are not uniform (6.35 N by the index and 4.7 N by the middle finger), as expected. The grip force exerted by the hand is in close range to the levels required for activities of daily living, as determined in a study for the evaluation of the prosthetic hand "Frederica" [57], though it is attributed to power grasp. Again, the maximum penetration achieved by the fingers after optimization is ~3.3 mm, which is less in comparison to the limiting conditions for the constraints given in Table V.

As mentioned above, the Grasp Energy required for executing the Grasp phase after optimization is about 55.9 mJ, while the Grasp Energy obtained from the simulation in MSC.Adams® is 73.6 mJ. This reduction in the energy required to execute the Grasp phase proves the efficacy of the developed grasp optimization algorithm.

8. Conclusions and Scope for Future Work

The present study successfully demonstrates a novel grasp optimization algorithm, in which the information of grasp trajectory obtained from a remotely located user can be used to move a robotic gripper

in an identical path. The optimization procedure minimizes the Grasp Energy-based objective function and determines an optimal distribution of contact forces subject to equality and inequality constraints. The optimization algorithm also introduces an instantaneous IK algorithm, which provides solutions for a robotic manipulator with multiple end-effectors, given that neither of the target task-space trajectories exceed its joint limits. A humanoid robotic hand model has been used to demonstrate the efficacy of the algorithm, and the results have been compared with CAD model simulated in MSC.Adams®, keeping all the conditions similar.

The results obtained by executing the optimization algorithm reveals that the algorithm can obtain a desirable contact force configuration, to counteract known external forces acting on the object. Using the configuration, locally optimal cartesian trajectories can be selected for each finger, such that traversing them consumes the least net energy by the gripper, for a given set of contact points. This implies that, even though the energy consumed by any one finger may not be optimal, the net energy consumed by the entire gripper for securing the grasp is the minimum for that set of contact points. It is seen that utilizing the grasp optimization algorithm in analytical approach reduces the energy to grasp an object and is less compared to that computed in numerical approach using MSC.Adams® solver. Again, due to arbitrary positioning of the hand, the contact force distribution that counteracts the gravitational force of the object is asymmetric, with the index finger and thumb carrying the majority of the load.

Further, in the present study, the described robotic humanoid hand is a theoretical model for the purposes of implementing the optimization algorithm. The comparison with the simulated data in MSC.Adams® has paved a way for further design iterations with the proposed algorithm aiming at mechanical designs of the robotic hand with twenty DoFs along with the selection of suitable actuators for the same to achieve optimal motion of gripper fingers (each four DoFs). Future work will also focus on finger-tip and object interaction, taking into account surface area of contact instead of the simple point-to-point contact modeled in the present study. This will help in describing a more accurate behavior of the fingers upon contact. Further, the choice of impact acceleration (Grasp phase) for calculation of the Grasp Energy is limited to a constant value. The effect of time-dependent linear and nonlinear Grasp phase acceleration profiles needs to be explored.

In the present study, the computation is carried out offline, that is, the optimization algorithm is separately executed based on pre-determined operating conditions, and the results are implemented on the robot hand model. Future work in this study entails the development of active force control algorithms with more efficient solutions, based on advanced optimization methods that can be used online for real-time implementation in humanoid robotic hand for grasping of rigid objects, while allowing grasps with a larger number of contact points, such as in power grasps.

Competing Interests Declaration. The author(s) declare none.

References

1. E. P. Gardner, K. S. Babu, S. D. Reitzen, S. Ghosh, A. S. Brown, J. Chen, A. L. Hall, M. D. Herzlinger, J. B. Kohlenstein and J. Y. Ro, "Neurophysiology of Prehension. I. Posterior Parietal Cortex and Object-Oriented Hand Behaviors," *J. Neurophysiol.* **97**(1), 387–406 (2007).
2. B. Zhang, Y. Xie, J. Zhou, K. Wang and Z. Zhang, "State-of-the-Art Robotic Grippers, Grasping and Control Strategies, as Well as Their Applications in Agricultural Robots: A Review," *Comput. Electron. Agric.* **177**(July) (2020).
3. D. W. Marhefka and D. E. Orin, "A Compliant Contact Model with Nonlinear Damping for Simulation of Robotic Systems," *IEEE Trans. Syst. Man, Cybern. - Part A Syst. Humans* **29**(6), 566–572 (1999).
4. Fan-Tien Cheng and D. E. Orin, "Optimal Force Distribution in Multiple-Chain Robotic Systems," *IEEE Trans. Syst. Man. Cybern.* **21**(1), 13–24 (1991).
5. Ki Suh and J. Hollerbach, "Local versus Global Torque Optimization of Redundant Manipulators," *Proceedings. 1987 IEEE International Conference on Robotics and Automation* (1987) pp. 619–624.

6. H.-J. Kang and R. A. Freeman, "Joint Torque Optimization of Redundant Manipulators via the Null Space Damping Method," *Proceedings 1992 IEEE International Conference on Robotics and Automation* (2003) pp. 520–525.

7. J. Hollerbach and Ki Suh, "Redundancy Resolution of Manipulators through Torque Optimization," *IEEE J. Robot. Autom.* **3**(4), 308–316 (1987).

8. R. V. Dubey, J. A. Euler and S. M. Babcock, "An Efficient Gradient Projection Optimization Scheme for a Seven-Degree-of-Freedom Redundant Robot with Spherical Wrist," *Proceedings. 1988 IEEE International Conference on Robotics and Automation* (2003) pp. 28–36.

9. K. Y. Tsai and D. Kohli, "Trajectory Planning in Task Space for General Manipulators," *J. Mech. Des. Trans. ASME* **115**(4), 915–921 (1993).

10. P. Gorce, C. Villard and J. G. Fontaine, "Grasping, Coordination and Optimal Force Distribution in Multifingered Mechanisms," *Robotica* **12**(3), 243–251 (1994).

11. S. H. Bakhy, "Modeling of Contact Pressure Distribution and Friction Limit Surfaces for Soft Fingers in Robotic Grasping," *Robotica* **32**(7), 1005–1015 (2014).

12. D. Jeong, I. Jo and J. Bae, "Analysis on the Force Distribution of Various Grasps for the Design of a Hand Exoskeleton," *2014 11th International Conference on Ubiquitous Robots and Ambient Intelligence, URAI 2014* (2014) pp. 127–131.

13. I. Jo and J. Bae, "Design and Control of a Wearable and Force-Controllable Hand Exoskeleton System," *Mechatronics* **41**, 90–101 (2017).

14. H.-J. Kang, "Stable Joint Torque Optimization for Multiple Cooperating Redundant Manipulator System," *KSME J.* **9**(1), 102 (1995).

15. Y. Zhang, S. S. Ge and T. H. Lee, "A Unified Quadratic-Programming-Based Dynamical System Approach to Joint Torque Optimization of Physically Constrained Redundant Manipulators," *IEEE Trans. Syst. Man Cybern. Part B* **34**(5), 2126–2132 (2004).

16. C. A. Klein and S. Kittivatcharapong, "Optimal Force Distribution for the Legs of a Walking Machine with Friction Cone Constraints," *IEEE Trans. Robot. Autom.* **6**(1), 73–85 (1990).

17. M. Buss, H. Hashimoto and J. B. Moore, "Dextrous Hand Grasping Force Optimization," *IEEE Trans. Robot. Autom.* **12**(3), 406–418 (1996).

18. J. S. Dai and D. R. Kerr, "Analysis of Force Distribution in Grasps Using Augmentation," *Proc. Inst. Mech. Eng. Part C J. Mech. Eng. Sci.* **210**(1), 15–22 (1996).

19. M. Suhaib, R. A. Khan and S. Mukherjee, "Contact Force Optimization for Stable Grasp of Multifingire Robotic Grippers," *Proceedings of the World Congress on Engineering 2011, WCE 2011* (2011) pp. 2194–2197.

20. P. Jia, W. li Li, G. Wang and S. Y. Li, "Optimal Grasp Planning for a Dexterous Robotic Hand Using the Volume of a Generalized Force Ellipsoid during Accepted Flattening," *Int. J. Adv. Robot. Syst.* **14**(1) (2017).

21. Yong Yu, K. Takeuchi, and T. Yoshikawa, "Optimization of Robot Hand Power Grasps," *Proceedings. 1998 IEEE International Conference on Robotics and Automation (Cat. No.98CH36146)* (1998) pp. 3341–3347.

22. M. B. Horowitz and J. W. Burdick, "Combined Grasp and Manipulation Planning as a Trajectory Optimization Problem," *2012 IEEE International Conference on Robotics and Automation* (2012) pp. 584–591.

23. H. Dong, E. Asadi, C. Qiu, J. Dai and I. M. Chen, "Grasp Analysis and Optimal Design of Robotic Fingertip for Two Tendon-Driven Fingers," *Mech. Mach. Theory* **130**, 447–462 (2018).

24. Y. Fan and M. Tomizuka, "Efficient Grasp Planning and Execution With Multifingered Hands by Surface Fitting," *IEEE Robot. Autom. Lett.* **4**(4), 3995–4002 (2019).

25. A. Müller, M. Aydemir, A. Glodde and F. Dietrich, "Design Approach for Heavy-Duty Soft-Robotic-Gripper," *Procedia CIRP* **91**, 301–305 (2020).

26. D. Kim, A. Li and J. Lee, "Stable Robotic Grasping of Multiple Objects Using Deep Neural Networks," *Robotica* **39**(4), 735–748 (2021).

27. S. A. Pertuz, C. H. Llanos and D. M. Munoz, "Development of a Robotic Hand Using Bioinspired Optimization for Mechanical and Control Design: UnB-Hand," *IEEE Access* **9**(1), 61010–61023 (2021).

28. N. Elangovan, L. Gerez, G. Gao and M. Liarokapis, "Improving Robotic Manipulation Without Sacrificing Grasping Efficiency: A Multi-Modal, Adaptive Gripper With Reconfigurable Finger Bases," *IEEE Access* **9**, 83298–83308 (2021).

29. B. Aceituno-Cabezas, J. Ballester and A. Rodriguez, "Certified Grasping," *arXiv preprint*, arXiv:1909.03985 (2019).

30. W. Yan, Z. Deng, J. Chen, H. Nie and J. Zhang, "Precision Grasp Planning for Multi-Finger Hand to Grasp Unknown Objects," *Robotica* **37**(08), 1415–1437 (2019).

31. T. Singh and S. Ambike, "A Soft-Contact and Wrench Based Approach to Study Grasp Planning and Execution," *J. Biomech.* **48**(14), 3961–3967 (2015).

32. H. Dong, C. Qiu, D. K. Prasad, Y. Pan, J. Dai and I.-M. Chen, "Enabling Grasp Action: Generalized Quality Evaluation of Grasp Stability via Contact Stiffness from Contact Mechanics Insight," *Mech. Mach. Theory* **134**, 625–644 (2019).

33. K. Mirza and D. E. Grin, "General Formulation for Force Distribution in Power Grasp," *Proceedings of the 1994 IEEE International Conference on Robotics and Automation* (2002) pp. 880–887.

34. T. Yoshikawa, T. Watanabe and M. Daito, "Optimization of Power Grasps for Multiple Objects," *Proceedings 2001 ICRA. IEEE International Conference on Robotics and Automation (Cat. No.01CH37164)* (2001) pp. 1786–1791.

35. E. Neha, M. Suhaib and S. Mukherjee, "Grasp Force Analysis of Four-Finger Tendon Actuated Robotic Hand," *Proceedings of the Advances in Robotics 2019* (2019) pp. 1–5.

36. S. Yao, M. Ceccarelli, G. Carbone and Z. Dong, "Grasp Configuration Planning for a Low-Cost and Easy-Operation Underactuated Three-Fingered Robot Hand," *Mech. Mach. Theory* **129**, 51–69 (2018).

37. F. Schmitt, O. Piccin, L. Barbé and B. Bayle, "Soft Robots Manufacturing: A Review," *Front. Robot. AI* **5**(JUN), 84 (2018).

38. I. Kapandji, "The Physiology of the Joints. Volume 2," *Postgrad. Med. J.* **51**(599), 682 (1975).
39. S. Cobos, M. Ferre, M. A. Sanchez Uran, J. Ortego and C. Pena, "Efficient Human Hand Kinematics for Manipulation Tasks," *2008 IEEE/RSJ International Conference on Intelligent Robots and Systems* (2008) pp. 2246–2251.
40. M. W. Spong, S. Hutchinson and M. Vidyasagar, *Robot Modeling and Control* (Wiley, 2005).
41. B. Buchholz and T. J. Armstrong, "An Ellipsoidal Representation of Human Hand Anthropometry," *Hum. Factors J. Hum. Factors Ergon. Soc.* **33**(4), 429–441 (1991).
42. B. Buchholz, T. J. Armstrong and S. A. Goldstein, "Anthropometric Data for Describing the Kinematics of the Human Hand," *Ergonomics* **35**(3), 261–273 (1992).
43. D. A. Winter, *Biomechanics and Motor Control of Human Movement* (John Wiley Sons Inc., Waterloo, Canada, 2009).
44. W. Xu, Z. Mu, T. Liu and B. Liang, "A Modified Modal Method for Solving the Mission-Oriented Inverse Kinematics of Hyper-Redundant Space Manipulators for on-Orbit Servicing," *Acta Astronaut.* **139**, 54–66 (2017).
45. L. Ren, J. K. Mills and D. Sun, "Adaptive Synchronization Control of a Planar Parallel Manipulator," *Proceedings of the 2004 American Control Conference* (2004) pp. 3980–3985 vol.5.
46. R. V. Ram, P. M. Pathak and S. J. Junco, "Inverse Kinematics of Mobile Manipulator Using Bidirectional Particle Swarm Optimization by Manipulator Decoupling," *Mech. Mach. Theory* **131**, 385–405 (2019).
47. G. Roy, S. Mukherjee, T. Das and S. Bhaumik, "Single Support Phase Gait Kinematics and Kinetics for a Humanoid Lower Limb Exoskeleton," *2020 IEEE Region 10 Symposium (TENSYMP)* (2020) pp. 138–141.
48. T. Feix, J. Romero, H. B. Schmiedmayer, A. M. Dollar and D. Kragic, "The GRASP Taxonomy of Human Grasp Types," *IEEE Trans. Human-Machine Syst.* **46**(1), 66–77 (2016).
49. S. Mukherjee and A. Mahapatra, "Compliant Contact Modeling of a Humanoid Robotic Thumb for Assisting Grasp," *2019 IEEE International Conference on Intelligent Systems and Green Technology (ICISGT)* (2019) pp. 94–98.
50. K. H. Hunt and F. R. E. Crossley, "Coefficient of Restitution Interpreted as Damping in Vibroimpact," *J. Appl. Mech.* **42**(2), 440 (1975).
51. K. L. Johnson, *Contact Mechanics* (Cambridge University Press, Cambridge, 1985).
52. J. J. Craig, *Introduction to Robotics* (Pearson Education International, 2005).
53. M. Svinin, K. Ueda and M. Kaneko, "On the Liapunov Stability of Multi-Finger Grasps," *Robotica* **18**(1), 59–70 (2000).
54. Y. L. Xiong, D. J. Sanger and D. R. Kerr, "Geometric Modelling of Bounded and Frictional Grasps," *Robotica* **11**(2), 185–192 (1993).
55. S. R. Buss, "Introduction to Inverse Kinematics with Jacobian Transpose, Pseudoinverse and Damped Least Squares Methods," *IEEE J. Robot. Autom.* **17**(16), 1–19 (2004).
56. B. Siciliano, L. Sciavicco, L. Villani and G. Oriolo, *Robotics* (Springer London, London, 2009).
57. D. Esposito, S. Savino, C. Cosenza, E. Andreozzi, G. D. Gargiulo, C. Polley, G. Cesarelli, G. D'Addio and P. Bifulco, "Evaluation of Grip Force and Energy Efficiency of the 'Federica' Hand," *Machines* **9**(2), 25 (2021).

Appendix: Grasp Optimization Algorithm

The grasp optimization algorithm developed in the present study has been summarized as follows:

A.1 The Objective Function

Minimize, $GE_{net} = \sum_{j=1}^{N} \sum_{i=1}^{L_j} \int_{t=t_I}^{t_F} (\rho + 1) \left(\lambda \dot{\delta} + K \right) \delta^\rho \mathrm{d}t,$

subject to,

$$0 \le \delta \le \delta_{max},$$

$$0 \le \dot{\delta} \le \dot{\delta}_I \le \dot{\delta}_{max},$$

$$-\left| \ddot{\delta}_{max} \right| \le \ddot{\delta} < 0,$$

$$0 < t_{I_{min}} \le t_I \le t_{I_{max}} < t_F,$$

$$\left\{ \sum_{j=1}^{N} \sum_{i=1}^{L_j} \vec{h}_{e_{ji}} \right\}_{t=t_F} + \vec{F}_e = 0,$$

$$-f_{ji}^x + \frac{\mu}{\sqrt{2}} F_{n_{ji}} < 0,$$

$$f_{ji}^x + \frac{\mu}{\sqrt{2}} F_{n_{ji}} < 0,$$

$$-f_{ji}^y + \frac{\mu}{\sqrt{2}} F_{ji} < 0,$$

$$f_{ji}^y + \frac{\mu}{\sqrt{2}} F_{n_{ji}} < 0.$$

A.2 Step-wise computation of the grasp optimization algorithm

Step 1: Selection of a time-based penetration acceleration profile, such that the impact acceleration lies within the range given in Eq. (13c), assuming $\ddot{\delta}_{max}$ is known. Here, the acceleration profile is arbitrarily chosen as a constant, a_1, satisfying the constraints ($a_1 < 0$).

Step 2: Selection of the initial time of impact t_I from the range given in Eq. (14), assuming $t_{I_{min}}$, $t_{I_{max}}$ and t_F are known.

Step 3: Integration of the penetration acceleration with respect to time, such that the penetration velocity profile is given by,

$$\dot{\delta} = a_1 t + c_1 \tag{20a}$$

Using the boundary condition, $\left\{\dot{\delta}\right\}_{t=t_F} = 0$, the instantaneous penetration velocity profile is given by,

$$\dot{\delta} = a_1 t - a_1 t_F \tag{21b}$$

Step 4: Calculation of the Impact velocity, given by,

$$\dot{\delta}_I = a_1 (t_I - t_F) \tag{22}$$

Step 5: Integration of the penetration velocity with respect to time, such that the penetration depth profile is given by,

$$\delta = \frac{a_1 t^2}{2} - (a_1 t_F)\, t + c_2. \tag{23a}$$

Using the boundary condition, $\{\delta\}_{t=t_I} = 0$, the instantaneous penetration depth profile is calculated as,

$$\delta = \frac{a_1 t^2}{2} - (a_1 t_F)\, t + \left(a_1 t_F t_I - \frac{a_1 t_I^2}{2} \right). \tag{24b}$$

Step 6: Determination of the value of $\dot{\delta}_I$ using Eq. (22) and check if the value is within the desired range given by Eq. (13b)).

Step 7: Evaluation of the Eq. (24b) at $t = t_F$, if the condition in step 6 is satisfied, to calculate the net penetration depth for the selected a_1 and t_I. Check if the value is within the range specified by Eq. (13a).

Step 8: Calculation of the normal force F_n at $t = t_F$, if the steps 6 and 7 are satisfied. Thus, substituting Eqs. (21b) and (24b) in Eq. (4):

$$F_n = \left(\lambda \left(\frac{a_1 t^2}{2} - (a_1 t_F)\, t + \left(a_1 t_F t_I - \frac{a_1 t_I^2}{2} \right) \right)^\rho \right) (a_1 t - a_1 t_F) + K \left(\frac{a_1 t^2}{2} - (a_1 t_F)\, t + \left(a_1 t_F t_I - \frac{a_1 t_I^2}{2} \right) \right)^\rho \tag{25}$$

Then, at $t = t_F$, for the boundary condition, $\{\dot{\delta}\}_{t=t_F} = 0$, Eq. (25) reduces to,

$$\{F_n\}_{t=t_F} = K^* \left(\frac{a_1}{2} (t_F - t_I)^2 \right)^\rho \tag{26}$$

Step 9: Calculation of the friction forces f_x and f_y, using the value of F_n obtained from Eq. (26) in step 8 by applying the bounds given in Eqs. (16a) – (16d). The friction forces in the local contact frame are calculated as:

$$f_x = \frac{k_1 \mu}{\sqrt{2}} F_n \tag{27a}$$

$$f_y = \frac{k_2 \mu}{\sqrt{2}} F_n \tag{27b}$$

where $k_1, k_2 \in (0,1)$.

Step 10: Satisfying the equilibrium condition for a multiple sets of friction forces, by varying the values of k_1 and k_2 using Eqs. (27a) and (27b). The force vector at a given point of contact turns out as:

$$\vec{h}_e = \left(\frac{k_1 \mu}{\sqrt{2}} F_n, \ \frac{k_2 \mu}{\sqrt{2}} F_n, \ F_n \right)^T \tag{28}$$

Step 11: Satisfying of the equilibrium constraint in Eq. (15) after computation of Eq. (28) for each contact point.

Step 12: Evaluation of the objective function, given by Eq. (12), if all the above-mentioned constraints are successfully satisfied for a given set of penetration acceleration coefficients and time of impact.

Step 13: Computation of the minimal value or the optimum value of Grasp-Energy, after successful evaluation of the steps 1 – 12, for each set of contact frictions, penetration acceleration and impact time values.

Step 14: Determination of the set of optimal parameters corresponding to step 13.

Step 15: Selection of the joint trajectories requiring minimum joint torque.

- Firstly, the Grasp phase inverse kinematics is performed for each Contact phase configuration solution, utilizing the optimal parameters determined in the previous steps. The procedures described in Section 6.1, by Eqs. (17a), (17b) and (18) are followed.
- Secondly, after determining the joint torque profiles for each trajectory solution, the Approach phase joint trajectories are generated using the procedures given in Section 6.2.
- Finally, the torque profiles for the possible Approach phase trajectories are determined.

Each corresponding solution of joint trajectories and torque profiles for both phases are concatenated. The complete joint torque profile, with the minimum infinity norm is selected, and the corresponding joint trajectory solution set is assigned as the optimal grasp trajectory.